High-Fidelity Multidisciplinary Design Optimization of Wing Shape for Regional Jet Aircraft

Kazuhisa Chiba[1], Shigeru Obayashi, Kazuhiro Nakahashi, and Hiroyuki Morino[2]

[1] Tohoku University, Katahira2-1-1, Aoba-ku, Sendai 980-8577, Japan,
chiba@edge.ifs.tohoku.ac.jp,
WWW home page: http://www.ifs.tohoku.ac.jp/edge/indexe.html
[2] Mitsubishi Heavy Industries, Ltd., Oye-cho 10, Minato-ku,
Nagoya 455-8515, Japan

Abstract. A large-scale, real-world application of Evolutionary Multi-Criterion Optimization (EMO) is reported in this paper. The Multidisciplinary Design Optimization among aerodynamics, structures and aeroelasticity for the wing of a transonic regional jet aircraft has been performed using high-fidelity models. An Euler/Navier-Stokes (N-S) Computational Fluid Dynamics (CFD) solver is employed for the aerodynamic evaluation. The NASTRAN, a commercial software, is coupled with a CFD solver for the structural and aeroelastic evaluations. Adaptive Range Multi-Objective Genetic Algorithm is employed as an optimizer. The objective functions are minimizations of block fuel and maximum takeoff weight in addition to difference in the drag between transonic and subsonic flight conditions. As a result, nine non-dominated solutions have been generated. They are used for tradeoff analysis among three objectives. One solution is found to have one percent improvement in the block fuel compared to the original geometry designed in the conventional manner. All the solutions evaluated during the evolution are analyzed by Self-Organizing Map to extract key features of the design space.

1 Introduction

Recent researches on Multidisciplinary Design Optimization (MDO) have been conducted for aircraft design[1, 2]. Pure aerodynamic optimization shows wings with a low thickness-to-chord ratio and a high aspect ratio. These wings suffer undesirable aeroelastic phenomena from the low bending and torsional stiffness. Aerostructural interacted optimization is needed to overcome these phenomena and to perform a realistic aircraft design[3]. This multi-criterion optimization will provide a good application field for EMO.

The project to develop a more environmentally suitable, highly efficient transonic regional jet aircraft has been founded by Ministry of Economy, Trade and Industry (METI) since 2003. Mitsubishi Heavy Industries, Ltd. (MHI) is the

prime contractor for the project. The aim of this project is to build a demonstrator with advanced technologies, such as low drag wing design, light weight composite structures which are necessary for reduction of environmental burden. The initial aircraft geometry has been obtained from a conventional design method.

The objective of this study is to optimize the three-dimensional wing shape for the proposed regional jet aircraft using evolutionary multi-objective optimization with high-fidelity simulations as a collaboration between Institute of Fluid Science (IFS), Tohoku University and MHI. From the optimization results, tradeoff analysis has been performed among the three objectives. Moreover, by using a data mining technique, the aerostructural design knowledge for transonic regional jet aircraft has been obtained.

In the present study, high-fidelity simulation tools such as Reynolds-averaged Navier-Stokes solver for aerodynamics, NASTRAN, a versatile and high-fidelity commercial software, for structures and aeroelasticity are coupled together for MDO. Although the Euler/N-S solver may be still too expensive for the real-world design environment, it will predict complex and nonlinear flow phenomena such as shock wave and separation more accurately. Such nonlinearity will provide a severe test case for EMO. With the aid of rapid progress in computer hardware, the demonstration in this paper will become a standard design practice soon.

2 Multidisciplinary Design Optimization

2.1 Objective Functions

In this study, because the target range for the regional jet is given, the minimization of the block fuel derived from aerodynamics and structures is selected as an objective function instead of the range maximization commonly used for aircraft design. The block fuel is defined as the minimum fuel mass for the fixed range. In addition, two more objective functions are considered as the minimization of the maximum takeoff weight and the minimization of the difference in the drag coefficient between transonic and subsonic flight conditions.

2.2 Geometry Definition

The design variables define the aerodynamic geometry. Structural optimization and aeroelastic transformation are performed using NASTRAN under the given aerodynamic geometry after aerodynamics, structures and flutter are evaluated, the objective functions are calculated.

The design variables are related to airfoil, twist and wing dihedral. The airfoil is defined at three spanwise cross sections using the modified PARSEC[4] with nine design variables (x_{up}, z_{up}, $z_{xx_{up}}$, x_{lo}, z_{lo}, $z_{xx_{lo}}$, α_{TE}, β_{TE} and $r_{LE_{lo}}/r_{LE_{up}}$) per cross section shown in Fig. 1. The twists are defined at six spanwise locations, and then wing dihedrals are defined at kink and tip locations. An entire wing

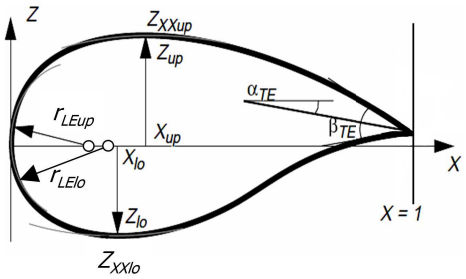

Fig. 1. Illustration of the modified PARSEC airfoil shape defined by nine design variables.

shape is thus defined by using 35 design variables. In this study, the geometry of each individual is generated by the unstructured dynamic mesh method[5, 6] using displacement from the initial geometry.

The five constraints are considered. The first three are about geometrical constraints and the last two are for the results as follows; 1) PARSEC works successfully. 2) Rear spar heights are greater than required for the housing of the control surfaces. 3) The lower and upper surfaces of the spars change monotonically in the spanwise direction. 4) The lift coefficients increase monotonically as Mach number increases. 5) The evaluated fuel for the given range is less than the wing fuel volume.

2.3 Optimizer

Evolutionary algorithms (EAs), in particular genetic algorithms (GAs), are based on the theory of evolution, where a biological population evolves over generations to adapt to an environment by selection, crossover and mutation. Fitness, individual and genes in the evolutionary theory correspond to an objective function, design candidate and design variables in design optimization problems, respectively.

GAs search the optimum from multiple points in the design space simultaneously and stochastically. GAs can prevent the search from settling in a local optimum. Moreover, GAs do not require computing gradients of the objective function. These features lead to the following advantages of GAs coupled with computational fluid dynamics (CFD): 1) GAs have the capability of finding global optimal solutions. 2) GAs can be processed in parallel. 3) High fidelity CFD codes can be adapted to GAs easily without any modification. 4) GAs are not sensitive to any noise that might be present in the computation.

Adaptive range multi-objective genetic algorithm (ARMOGA)[7] is an efficient multi-objective evolutionary algorithm (MOEA) designed for aerodynamic optimization and multidisciplinary design optimization problems using high-fidelity CFD solvers with a large computational time. ARMOGA has the range

adaptation based on population statistics, and the population is re-initialized at every N generations so that the search region adapts toward promising regions.

In the present ARMOGA, fitness value of each solution is determined by Fleming and Fonseca's Pareto-ranking method coupled with fitness sharing approach[8]. Each individual is assigned a rank according to the number of individuals dominating it. The assigned fitness values are divided by the niche count, which is calculated by summing the sharing function values. To find the Pareto solutions more effectively, the so-called best-N selection[9] is also implemented. After shared fitness values are determined for all individuals, the stochastic universal selection (SUS)[10] is applied to select better solutions for producing a new generation. Blended crossover (BLX-α)[11] and polynomial mutation methods[12] are adopted for crossover and mutation.

The advantages of ARMOGA are the following: It is possible to obtain the non-dominated solutions efficiently because of the concentrated search of the probable design space. It also produces diversified solutions.

2.4 Evaluation Method

The optimizer generates eight individuals per generation, and evaluates aerodynamic and structural properties of each one as follows. 1) Structural optimization is performed to realize minimum wing weight with constraints of flutter and strength requirements. 2) Static aeroelastic analysis is performed at three flight conditions to determine the aeroelastic deformed shapes by Euler solver. 3) Aerodynamic evaluations are performed for the aeroelastic deformed shapes using Navier-Stokes solver. 4) Flight envelope analysis is performed using the above obtained properties to evaluate objective functions by N-S solver. Using objective functions evaluated, the optimizer generates new individuals for the next generation via genetic operations such as selection, crossover and mutation.

In the present study, MSC. NASTRAN^{TM}[13] which is a high-fidelity commercial software is employed for the structural and aeroelastic evaluations. Detailed structural model was provided by MHI. Besides, the unstructured mesh method[14, 15] is used to evaluate aerodynamic performance. The Euler equations are computed for structural optimization and aeroelasticity. The three-dimensional Reynolds-averaged Navier-Stokes (RANS) equations are computed with a finite-volume cell-vertex scheme. The unstructured hybrid mesh method[16] is applied to capture the boundary layer accurately and efficiently. The Harten-Lax-van Leer-Einfeldt-Wada Riemann solver[17] is used for the numerical flux computations. The Venkatakrishnan's limiter[18] is applied when reconstructing second order accuracy. The lower-upper symmetric-Gauss-Seidel implicit scheme[19] is applied for time integration.

Considering a turbulence model, the Spalart-Allmaras one-equation model modified by Dacles-Mariani *et al.*[20] is employed without transition. This model is confirmed to be effective for capturing the complex vortex structure[21].

Euler and RANS computations are carried out at subsonic and transonic flight conditions, respectively. Taking advantage of the parallel search in EAs,

the present optimization is parallelized on vector-parallel machines NEC SX-5 and SX-7. The master processing element (PE) manages ARMOGA, while the slave PEs compute aerostructural evaluation processes. Slave processes do not require synchronization.

3 Optimization Results

The population size is set to eight, and then roughly 70 Euler and 90 RANS computations are performed in one generation. It takes roughly one hour and nine hours of CPU time of NEC SX-5 and SX-7 one PE for Euler and RANS computations, respectively. The population is re-initialized at every five generations for the range adaptation. The total evolutionary computation of 16 generations is carried out so far. The evolution may not converge yet. However, the result is satisfactory, because several non-dominated solutions achieve significant improvements over the initial design. Furthermore, enough number of solutions have been searched so that the sensitivity of the design space around the initial design can be analyzed. This will provide useful information for designers.

All solutions evaluated are shown in Fig. 2, and Fig. 3 shows all solutions projected on two dimensional plane between two objectives, the block fuel and the drag divergence. As this figure shows that the non-dominated front is generated, there is tradeoff between the block fuel and the drag divergence.

Although the wing box weight, on the whole, tends to increase compared with that of the initial geometry, the block fuel can be also reduced. It means that aerodynamic performance can redeem the penalty due to the structural weight. An individual, indicated as 'optimized', on the non-dominated front shown in Fig. 3 is picked up, and then optimized geometry is compared with the initial geometry. Figure 4 shows the comparison of polar curves. Although the corresponding the drag minimization is not considered here, this figure shows that the drag coefficients tend to reduce on the whole. Comparing the polar curves at the constant lift coefficient for the cruising condition, the drag coefficient of the optimized geometry has been found to be reduced 5.5 counts. Due to the drag improvement, the block fuel of the optimized geometry can be decreased over one percent even with its structural weight penalty.

Next, the mechanism of the drag reduction is investigated. Figure 5 shows the comparison of the spanwise distributions of lift and drag coefficients of initial and optimized geometries. This figure shows that the drag decreases at the 35.0 % spanwise location. Figure 6 shows the comparison of the pressure distributions at the 35.0 % spanwise location. This figure shows that the variation of the leading-edge bluntness works to depress the shock wave on the upper wing surface, namely, to reduce the wave drag. In fact, the pressure drag coefficient is reduced by 5.6 counts. Figure 7 shows the comparison of shock wave visualized by the shock function F_{shock}[22] which is given as follows,

$$F_{\mathrm{shock}} = \frac{\boldsymbol{V} \cdot \nabla P}{a \cdot |\nabla P|} \tag{1}$$

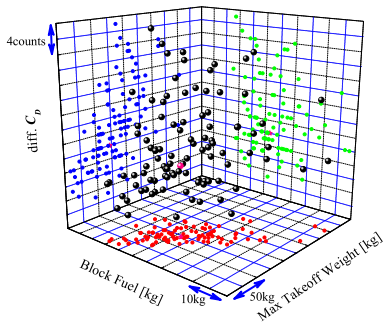

Fig. 2. All solutions plotted in three dimensional space of all objective function.

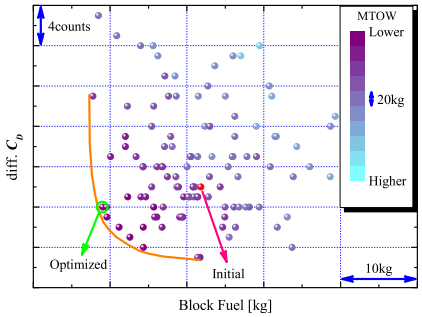

Fig. 3. All solutions on two dimensional plane between block fuel and drag divergence.

where $\boldsymbol{V}$ is velocity vector, P is pressure and a denotes the local speed of sound. The shock wave of the optimized geometry is weaker than the initial geometry in the vicinity of the 35.0 % spanwise location shown in Fig. 7. This fact signify the wave drag reduction. Moreover, the vorticity of wing wake of the optimized geometry in the vicinity of the 35.0 % spanwise location is weaker than of initial geometry shown by helicity contours in Fig. 8. Therefore, these figures show that the shape near the 35.0 % spanwise location, namely, the shape in the vicinity of the kink location has been found effective to reduce the drag.

4 Data Mining

If the optimization problem has only two objectives, tradeoffs can be visualized easily. However, if there are more than two objectives, the technique to visualize the computed non-dominated solutions is desired[23]. Therefore, in the present study, Self-Organizing Maps (SOMs) suggested by Kohonen[24] have been employed. SOM is not only the technique for the visualization but also the application tool for the intelligent compression of the information. In other words, SOM can be applied for the data mining technique to acquire the knowledge about design space. In this study, Viscovery® SOMine[25] produced by Eudaptics GmbH in Austria is employed.

4.1 Self-Organizing Map

Although SOMine is based on the SOM concept and algorithm, it employs an advanced variant of unsupervised neural networks, *i.e.* Kohonen's Batch-SOM.

The algorithm consists of two steps that are iteratively repeated until no more significant changes occur. First the distances between all data items $\{\boldsymbol{x}_i\}$ and the model vectors $\{\boldsymbol{m}_j\}$ are computed and each data item $\boldsymbol{x}_i$ is assigned to the unit c_i that represents it best.

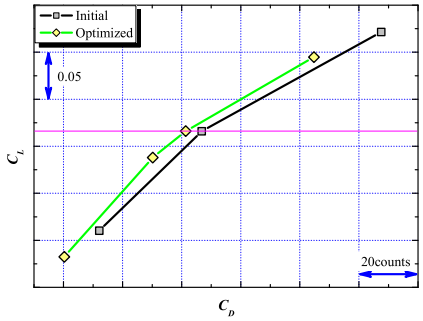

Fig. 4. Comparison of the polar curves between initial and optimized geometries.

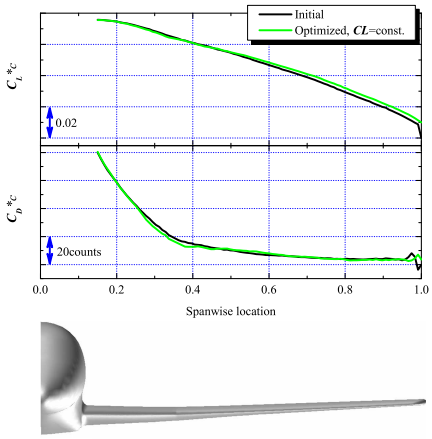

Fig. 5. Comparison of the lift and drag coefficients spanwise distributions between initial and optimized geometries.

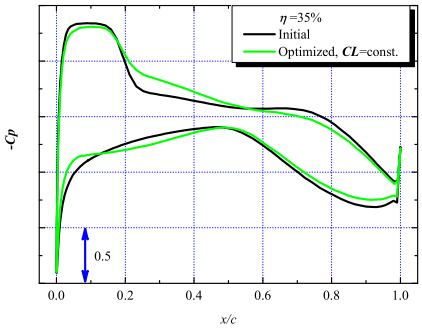

Fig. 6. Comparison of the pressure distributions and airfoil shapes between initial and optimized geometries at 35 % spanwise location.

Fig. 7. Comparison of shock wave visualizations colored by entropy at the transonic cruise flight condition between initial (left) and optimized (right) geometries.

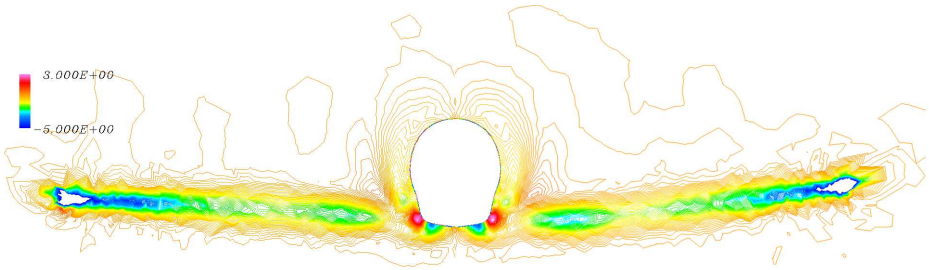

Fig. 8. Comparison of helicity contours of wing wake at the transonic cruise flight condition between initial (left) and optimized (right) geometries.

In the second step, each model vector is adapted to better fit the data it represents. To ensure that each unit j represents similar data items as its neighbors, the model vector $\boldsymbol{m}_j$ is adapted not only according to the assigned data items but also in regard to those assigned to the units in the neighborhood. The neighborhood relationship between two units j and k is usually defined by a Gaussian-like function

$$h_{jk} = \exp\left(-\frac{d_{jk}^2}{r_t^2}\right) \tag{2}$$

where d_{jk} denotes the distance between the units j and k on the map, and r_t denotes the neighborhood radius which is set to decrease with each iteration t.

Assuming a Euclidean vector space, the two steps of the Batch-SOM algorithm can be formulated as

$$c_i = \arg\min \|\boldsymbol{x}_i - \boldsymbol{m}_j\| \tag{3a}$$

$$\boldsymbol{m}_j^* = \frac{\sum_i h_{jc_i} \boldsymbol{x}_i}{\sum_i h_{jc_i}} \tag{3b}$$

where $\boldsymbol{m}_j^*$ is the updated model vector.

In contrast to the standard Kohonen algorithm, which makes a learning update of the neuron weights after each record being read and matched, the Batch-SOM takes a 'batch' of data, typically all records, and performs a 'collected' update of the neuron weights after all records have been matched. This is much like 'epoch' learning in supervised neural networks. The Batch-SOM is a more robust approach, since it mediates over a large number of learning steps. Most important, no learning rate is required. The SOMine implementation combines four enhancements to the plain Batch-SOM algorithm[26]. In SOMine, the uniqueness of the map is ensured by the adoption of the Batch-SOM and the linear initialization for input data.

Much like some other SOMs[27], SOMine creates a map in a two-dimensional hexagonal grid. Starting from numerical, multivariate data, the nodes on the

grid gradually adapt to the intrinsic shape of the data distribution. Since the order on the grid reflects the neighborhood within the data, features of the data distribution can be read off from the emerging map on the grid.

In SOMine, the trained SOM is systematically converted into visual information. The tool provides an extensive built-in capability for both pre-processing and post-processing as well as for the automatic colorcoding of the map and its components. SOMine is particularly useful in the determination of dependencies between variables as well as in the analysis of high-dimensional cluster distributions.

4.2 Cluster Analysis

Once SOM projects input space on a low-dimensional regular grid, the map can be utilized to visualize and explore properties of the data. When the number of SOM units is large, tofacilitate quantitative analysis of the map and the data, similar units need to be grouped, *i.e.*, clustered. The two-stage procedure — first using SOM to produce the prototypes which are then clustered in the second stage — was reported to perform well when compared to direct clustering of the data[27].

Hierarchical agglomerative algorithm is used for clustering here. The algorithm stats with a clustering where each node by itself forms a cluster. In each step of the algorithm two clusters are merged: those with minimal distance according to a special distance measure, the SOM-Ward distance[25]. This measure takes into account whether two clusters are adjacent in the map. This means that the process of merging clusters is restricted to topologically neighbored clusters. The number of clusters will be different according to the hierarchical sequence of clustering. A relatively small number will be chosen for visualization, while a large number will be used for generation of codebook vectors for respective design variables.

4.3 Tradeoff Analysis and Data Mining of the Design Space

All of the solutions have been projected onto the two-dimensional map of SOM. Figure 9 shows the resulting SOM with 10 clusters considering the three objectives. Furthermore, Fig. 10 shows the SOMs colored by the three objectives and three characteristic parameters, respectively. These color figures show the SOM shown in Fig. 9 can be grouped as follows: Upper left corner corresponds to the designs with high block fuel and maximum takeoff weight. Lower left corner corresponds to the designs with low block fuel and high drag divergence. Figure 10(a) and Fig. 10(c) show that there is a tradeoff between these two objective functions. Lower center area corresponds to the designs with low block fuel. Right hand side corresponds to the designs with low drag divergence. As Fig. 10(a) is similar coloring to Fig. 10(b), there is not a severe tradeoff between the block fuel and the maximum takeoff weight. Lower right corner corresponds to the designs with low of all objectives. Extreme non-dominated solutions are indicated in Fig. 10(a) to (c). Because they are in the different clusters, the

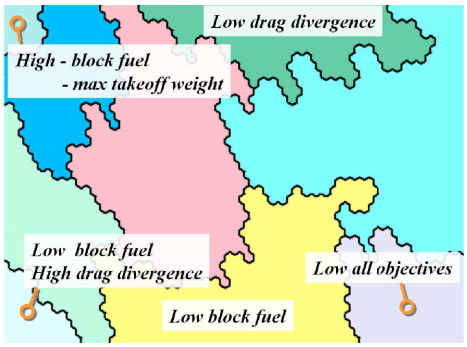

Fig. 9. SOM of all solutions in the three deimensional objective function space.

simultaneous optimization of the three objectives is impossible. However, the lower right cluster has relatively low values for all three objectives. This region of the design space may provide a sweet-spot for the present design problem.

Figure 10(d) shows the SOM colored by the drag coefficient at the cruising flight condition, the lower value exists on the lower right corner. As this area clusters the designs with the low of all objectives, this fact inspires that all objectives can be optimized simultaneously while the drag at cruising flight condition is reduced. Furthermore, because the value of the maximum takeoff weight shown in Fig. 10(b) existing at a the similar location as in Fig. 10(d), the drag coefficient is found effective to reduce the maximum takeoff weight.

Figure 10(e) shows the SOM colored by the lift-to-drag ratio at the cruising flight condition, the lower value exists on the upper left corner. Because the higher value of the block fuel shown in Fig. 10(a) exists at a similar location, the lower lift-to-drag ratio is effective to increase the block fuel strictly. Furthermore, the higher value of lift-to-drag ratio exists on the lower area shown in Fig. 10(e). Because the lower value of the block fuel shown in Fig. 10(a) exist at a similar location, the higher lift-to-drag ratio is effective to decrease the block fuel. But, the higher value of the transonic lift-to-drag ratio is not necessarily effective to reduce the block fuel in Fig. 10(e) because the range of not only cruise but also of takeoff-to-landing is considered in this study.

Figure 10(f) shows the SOM colored by the angle between inboard and outboard on upper wing surface expressing the gull-wing at kink location. When this angle is greater/less than 180 deg, it means gull/inverted gull-wing. The characteristic inverted gull-wing shape is shown in Fig. 11. The location where the higher value exists shown in Fig. 10(f) corresponds to the position where the higher value of the drag coefficient at cruising flight condition shown in Fig. 10(d). However, when the angle is less than 180 deg, there is little correlation between Figs. 10(d) and (f). As it is known that the inverted gull-wing obtains structural weight increase, no-gull wing should be designed for structure and manufacture.

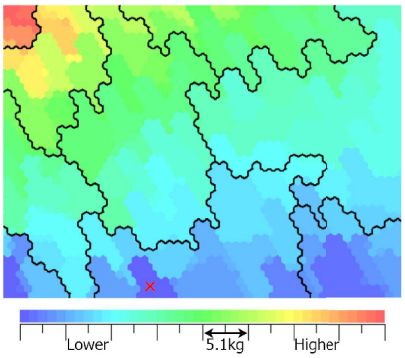

(a) SOM colored by the block fuel as the objective function 1

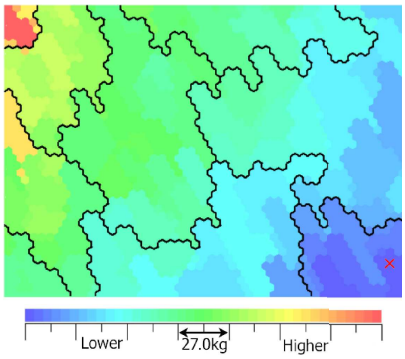

(b) SOM colored by the maximum takeoff weight as the objective function 2

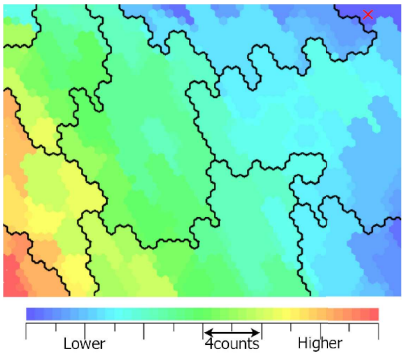

(c) SOM colored by the drag divergence as the objective function 3

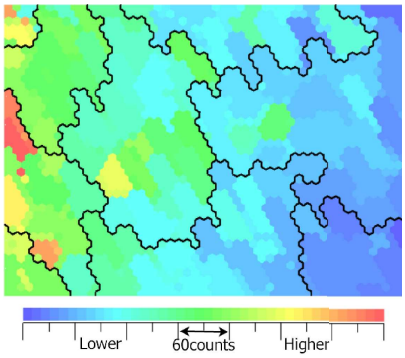

(d) SOM colored by the drag coefficient at the cruising flight condition

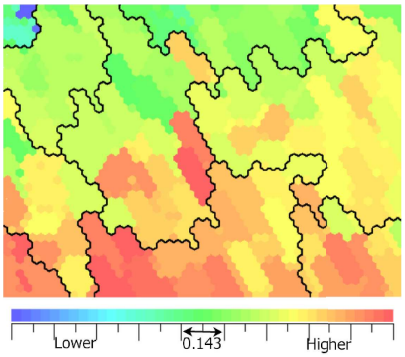

(e) SOM colored by the lift-to-drag ratio at the cruising flight condition

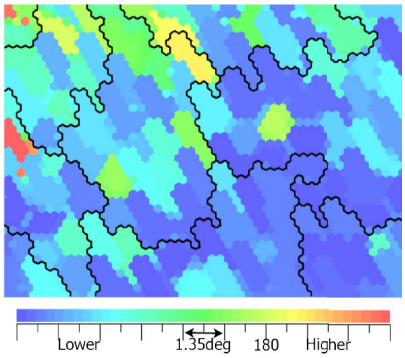

(f) SOM colored by the angle on upper surface expressing the gull-wing at kink location

Fig. 10. SOM colored by the objective functions and the characteristic values. The symbol × denotes the respective extreme non-dominated solutions in (a), (b) and (c).

Fig. 11. Visualization of a characteristic inverted gull-wing.

Finally, Fig. 12 shows the SOM colored by the characteristic design variables. Figure 12(a) shows the SOM colored by the design variable of PARSEC x_{up} at the 55.5 % spanwise location. When this value is increased in Fig. 12(a), the transonic drag is increased simultaneously shown in Fig.10(d). This means that the value of PARSEC x_{up} at the 55.5 % spanwise location has influence upon the transonic drag increase. Figures 12(b) and (c) show the SOMs colored by the design variables of PARSEC $r_{LE_{lo}}/r_{LE_{up}}$ at the 35.0 % spanwise location and PARSEC $z_{xx_{lo}}$ at the 55.5 % spanwise location, respectively. The decrease value of $r_{LE_{lo}}/r_{LE_{up}}$ and the increase value of $z_{xx_{lo}}$ in Figs. 12(b), (c) have influence upon the transonic lift-to-drag ratio decrease simultaneously shown in Fig. 10(e).

Figures 12(d), (e) and (f) show the SOMs colored by the design variables of the twist at the 35.0 %, 55.5 % and 96.0 % spanwise location, respectively. The geometry near the 55.5 % spanwise location does not improve largely about angle of attack shown in Fig. 12(e). The geometry near the 96.0 % spanwise location improves the twist up. In reverse, the geometry near the 35.0 % spanwise location improves the twist down. The improvement in the vicinity of the 35.0 % spanwise location is to restrain shock wave, namely, to reduce wave drag shown in Fig. 7. When the drag decreases, the lift may decrease simultaneously. The lift is increased to compensate for the reduction in the vicinity of kink location so that the angle of attack of the outboard wing is increased and roughly set to zero. It is noted that the angle of attack near the kink location is effective to the transonic drag especially as shown in Fig. 12(d). This fact corresponds to the phenomena visualized in Fig. 7. Specifically, as the shock wave which arises in the vicinity of the kink location is weaken, the angle of attack near the outboard wing with twist up is replaced and lost lift is made up to replace the angle of attack with twist down so that wave drag reduces. Twist up at outboard wing has no influence for transonic drag shown in Fig. 12(f). The other design variables are not found effective to reduce the objective functions and to increase aerodynamic performance as drag and lift-to-drag ratio at transonic cruise flight condition. Data mining technique using SOM has been found to be able to classify the design variables considering the influence upon the objectives and the aerodynamic performance.

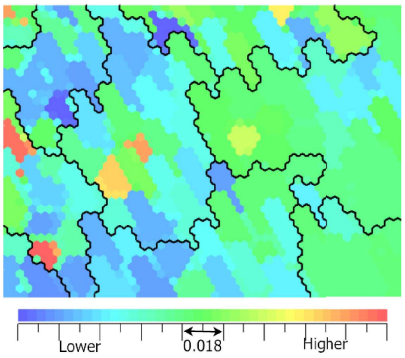

(a) SOM colored by the design variable of PARSEC x_{up} at the 55.5 % spanwise location

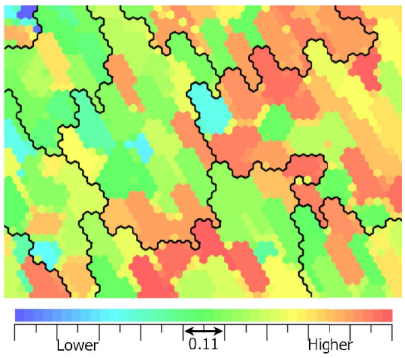

(b) SOM colored by the design variable of PARSEC $r_{LE_{lo}}/r_{LE_{up}}$ at the 35.0 % spanwise location

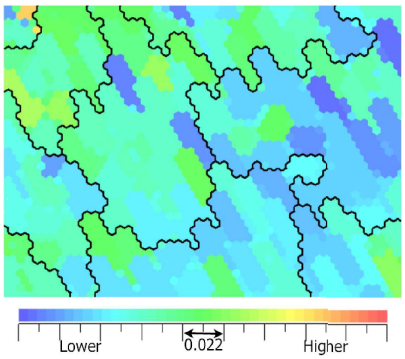

(c) SOM colored by the design variable of PARSEC $z_{xx_{lo}}$ at the 55.5 % spanwise location

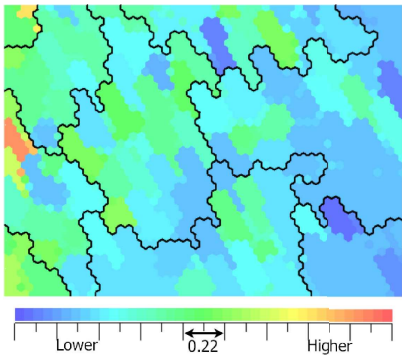

(d) SOM colored by the design variable of the twist angle at the 35.0 % spanwise location

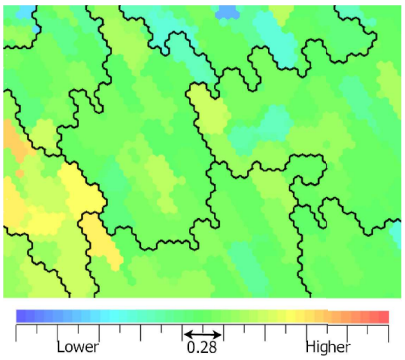

(e) SOM colored by the design variable of the twist angle at the 55.5 % spanwise location

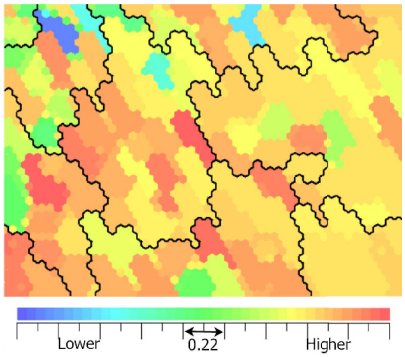

(f) SOM colored by the design variable of the twist angle at the 96.0 % spanwise location

Fig. 12. SOM colored by the characteristic design variables.

5 Conclusion

The wing shape of a regional jet aircraft has been optimized using Multidisciplinary Design Optimization techniques considering three aerostructural objective functions with high-fidelity evaluation and Adaptive Range Multi-Objective Genetic Algorithm. Consequently, the objective function value considering block fuel has been reduced over one percent compared with the initial geometry. The geometry change at the kink location has been found effective for the drag reduction. The tradeoff information among three objective functions has been revealed, and a tradeoff has been found between the block fuel and the drag divergence. Moreover, data mining for the design space has been performed using Self-Organizing Map. Therefore, the particular design variables have been found effective to reduce the objective functions and aerodynamic performance. Detailed observation of SOM reveals there is a sweet-spot in the design space where the three objectives become relatively low. The data mining technique provides knowledge about the design space, which is considered an important facet of solving optimization problems.

Acknowledgements

We would like to thank Mr. Takano, Y., graduate student of Tohoku University for generating the CATIA STL and the mesh data of the initial geometry. The Navier-Stokes computations were performed using NEC SX-5 in the Institute of Fluid Science, Tohoku University, and NEC SX-7 in Super-Computing System Information Synergy Center, Tohoku University.

References

1. Kroo, I., Altus, S., Braun, R., Gage, P., and Sobieski, I., "Multidisciplinary Optimization Methods for Aircraft Preliminary Design," AIAA Paper 94-4325-CP, 1994.
2. Sobieszczanski-Sobieski, J. and Haftka, R. T., "Multidisciplinary Aerospace Design Optimization: Survey of Recent Developments," *Structural Optimization*, Vol. 14, No. 1, 1997, pp. 1–23.
3. Martins, J. R. R. A., Alonso, J. J., and Reuther, J. J., "High-Fidelity Aerostructural Design Optimization of a Supersonic Business Jet," *Journal of Aircraft*, Vol. 41, No. 3, 2004, pp. 523–530.
4. Oyama, A., Obayashi, S., Nakahashi, K., and Hirose, N., "Aerodynamic Wing Optimization via Evolutionary Algorithms Based on Structured Coding," *Computational Fluid Dynamics Journal*, Vol. 8, No. 4, 2000, pp. 570–577.
5. Murayama, M., Nakahashi, K., and Matsushima, K., "Unstructured Dynamic Mesh for Large Movement and Deformation," AIAA Paper 2002-0122, 2002.
6. Yamazaki, W., Matsushima, K., and Nakahashi, K., "Aerodynamic Optimization of NEXST-1 SST Model at Near-Sonic Regime," AIAA Paper 2004-0034, 2004.
7. Sasaki, D., Obayashi, S., and Nakahashi, K., "Navier-Stokes Optimization of Supersunic Wings with Four Objectives Using Evolutionary Algorithm," *Journal of Aircraft*, Vol. 39, No. 4, 2002, pp. 621–629.

8. Fonseca, C. M. and Fleming, P. J., "Genetic Algorithms for Multiobjective Optimization: Formulation, Discussion and Generalization," *Proceedings of the Fifth International Conference on Genetic Algorithms*, 1993, pp. 416–423.
9. Obayashi, S., Takahashi, S., and Takeguchi, Y., "Niching and Elitist Models for MOGAs, Parallel Problem Solving from Nature," *PPSN V, Lecture Notes in Computer Science*, Springer, Berlin, Heidelberg, New York, 1998, pp. 260–269.
10. Baker, J. E., "Reducing Bias and Inefficiency in the Selection Algorithm," *Proceedings of the Second International Conference on Genetic Algorithms*, 1987, pp. 14–21.
11. Eshelman, L. J. and Schaffer, J. D., "Real-Coded Genetic Algorithms and Interval Schemata," *Foundations of Genetic Algorithms 2*, Morgan Kaufmann, San Mateo, CA, 1993, pp. 187–202.
12. Deb, K., *Multi-Objective Optimization Using Evolutionary Algorithms*, John Wiley & Sons, Ltd., Chichester, 2001.
13. "MSC. website," URL: http://www.mscsoftware.com/ [cited 14 September 2004].
14. Ito, Y. and Nakahashi, K., "Direct Surface Triangulation Using Stereolithography Data," *AIAA Journal*, Vol. 40, No. 3, 2002, pp. 490–496.
15. Sharov, D. and Nakahashi, K., "A Boundary Recovery Algorithm for Delaunay Tetrahedral Meshing," *Proceedings of the 5^{th} International Conference on Numerical Grid Generation in Computational Field Simulations*, 1996, pp. 229–238.
16. Ito, Y. and Nakahashi, K., "Improvements in the Reliability and Quality of Unstructured Hybrid Mesh Generation," *International Journal for Numerical Methods in Fluids*, Vol. 45, Issue 1, 2004, pp. 79–108.
17. Obayashi, S. and Guruswamy, G. P., "Convergence Acceleration of an Aeroelastic Navier-Stokes Solver," *AIAA Journal*, Vol. 33, No. 6, 1994, pp. 1134–1141.
18. Venkatakrishnan, V., "On the Accuracy of Limiters and Convergence to Steady State Solutions," AIAA Paper 93-0880, 1993.
19. Sharov, D. and Nakahashi, K., "Reordering of Hybrid Unstructured Grids for Lower-Upper Symmetric Gauss-Seidel Computations," *AIAA Journal*, Vol. 36, No. 3, 1998, pp. 484–486.
20. Dacles-Mariani, J., Zilliac, G. G., Chow, J. S., and Bradshaw, P., "Numerical/Experimental Study of a Wingtip Vortex in the Near Field," *AIAA Journal*, Vol. 33, No. 9, 1995, pp. 1561–1568.
21. Chiba, K., Obayashi, S., and Nakahashi, K., "CFD Visualization of Second Primary Vortex Structure on a 65-Degree Delta Wing," AIAA Paper 2004-1231, 2004.
22. Yamazaki, W., "Aerodynamic Optimization of Near-Sonic Plane Based on NEXST-1 SST Model," ICAS 2004-4.3.4, 2004.
23. Obayashi, S. and Sasaki, D., "Visualization and Data Mining of Pareto Solutions Using Self-Organizing Map," *EMO 2003, Lecture Notes in Computer Science*, Springer-Verlag Heidelberg, Faro, Portugal, 2003, pp. 796–809.
24. Kohonen, T., *Self-Organizing Maps*, Springer, Berlin, Heidelberg, 1995.
25. "Eudaptics website," URL: http://www.eudaptics.com [cited 16 June 2004].
26. Deboeck, G. and Kohonen, T., *Visual Explorations in Finance with Self-Organizing Maps*, London, Springer Finance, 1998.
27. Vesanto, J. and Alhoniemi, E., "Clustering of the Self-Organizing Map," *IEEE Transactions on Neural Networks*, Vol. 11, No. 3, 2000, pp. 586–600.